Spatial synchronization of regular optical patterns

R. Neubecker* and O. Jakoby
Institute of Applied Physics, Darmstadt University of Technology, Hochschulstrasse 6, 64289 Darmstadt, Germany
(Received 19 June 2002; revised manuscript received 13 March 2003; published 30 June 2003)

We investigate an extended, nonlinear optical experiment, exhibiting the spontaneous formation of hexagonal patterns out of a stationary bifurcation. The system is exposed to a two-dimensional spatially periodic forcing, namely, static hexagonal patterns, under variation of their spatial periodicity. Parameters are the strength of the forcing and the distance to pattern forming threshold. The system response is quantitatively characterized with different methods. We observe several locking regimes, where the system is entrained by the forcing. Most of the locking regimes can be related to resonances between the different critical wave numbers and the forcing wave number or its spatial harmonics. One particular locking appears to result from two of these simple resonances in a kind of generalized order m:n synchronization. The width of the locking regimes increases with forcing strength, apparently representing a spatial analog of Arnold tongues.

DOI: 10.1103/PhysRevE.67.066221 PACS number(s): 89.75.Kd, 47.54.+r, 42.65.Sf

I. INTRODUCTION

In nonlinear, spatially extended systems far from thermal equilibrium, spatial structures can develop spontaneously. It is an interesting question, how such systems respond to an external stimulus. We here consider a forcing by injecting a spatially structured signal. In certain instances, *synchronization* appears, i.e., the resulting system state corresponds to the injected structure. The investigations presented in this paper are connected to several fields of previous research. Before introducing our nonlinear-optical experiment, related properties of nonextended systems are summarized and work on extended nonoptical and optical systems is briefly reviewed.

The synchronization of two coupled oscillators is a well-known phenomenon, first described by Christiaan Huygens in 1665 for pendulum clocks. Detailed investigations on the response of nonlinear oscillators, subject to a periodic forcing, revealed that these not only lock onto a periodic external signal close to their own generic frequency ω_0 but can also be entrained by other frequencies ω', being a rational multiple with a *winding number* $m/n=\omega'/\omega_0$. The bandwidth of such a nonlinear resonance increases with the forcing strength—these bands of entrainment are called *Arnold tongues* [1]. Today, research on oscillators focuses on the synchronization of chaotic oscillators and the possible use for secure communication [1,2].

According to their additional degrees of freedom, spatially extended systems show a much wider spectrum of self-organization phenomena than single nonlinear oscillators. Spontaneous formation of spatiotemporal structures is investigated in many different areas [3–5]—from biology over chemistry to different fields of physics, such as fluid dynamics, plasma physics, solid state physics, and nowadays even in nonlinear optics [6]. When a control parameter exceeds a certain threshold, various simple spatial structures are observed to spontaneously evolve in such systems. Mostly these turn into complex, very dynamic states (*turbulence*) under further increase of the control parameter. To establish a bridge to the purely temporal phenomena, discrete systems such as coupled maps or coupled oscillators are investigated. In the following, we will instead focus on continuous systems.

External forcing of extended systems has been investigated in a variety of configurations. The focus is on two classes, namely, convection patterns and chemical reaction-diffusion systems. The largest part of the literature on this topic is theoretical or numerical, starting with spatially one-dimensional forcing of spatially one-dimensional systems [7–13]. In this context, analogies between spatial and temporal nonlinear resonances were pointed out [11]. Moreover, it was described that forcing can cause the formation of quasiperiodic structures, induced dynamics, the appearance of defects, or of spatial chaos. The state until the early nineties is summarized in the book by Walgraef [5].

Theories were then extended to particular cases of two-dimensional systems [14], and also to two-dimensional forcing [15]. Since there are many combinations of possibly coexisting spatial and temporal instabilities, and correspondingly a large variety of spontaneous spatiotemporal phenomena, so far no general theoretical treatment exists. Recent work goes beyond periodic forcing and focuses on the possibility to synchronize and control spatially chaotic systems—so far mostly in one-dimensional model equations [16–18].

Experimentally, forcing of a spatially continuous system is quite demanding, when the system quantities to be modulated in space and time are flow fields, temperature profiles, or distributions of chemical compounds. It is simpler to apply a spatially uniform, time-periodic forcing, which has been found to significantly alter the spatial structures [19–23]. Other variants of low-dimensional forcing are manipulations at discrete locations only [24] or by modulating the sidewalls [25].

One possibility to implement the two-dimensional spatial forcing is to structure the system itself, e.g., the boundary conditions in the third spatial dimension. Examples are the design of electrodes [26], the thickness of a liquid layer [27], the structuring of a catalytic surface [24,28,29], or the struc-

*Email address: ralph.neubecker@physik.tu-darmstadt.de

ture of a heated surface [30]. Since all these are fixed mechanical geometries, a continuous variation of forcing parameters, such as the spatial scale or the forcing strength, is difficult.

Early experiments with such a fixed forcing were performed on electrohydrodynamic convection rolls in a quasi-one-dimensional geometries [26], inspiring many of the following theoretical papers. Here, the system could use the second spatial dimension to adapt to the one-dimensional forcing. Fully two-dimensional forcing of two-dimensional systems was performed in a Belousov-Zhabotinsky reaction [28], in Bénard-Marangoni convection [30], and in catalytic oxidation of carbon monoxide [24,29].

Photosensitive systems offer much more experimental flexibility, because light waves can carry almost arbitrary spatial and temporal profiles. An optical forcing has been successfully used in photosensitive chemical reactions [31–35]. Here we will make use of optical forcing in a nonlinear optical system, where the light intensity itself is a central physical quantity.

The choice of the spatial distribution of the forcing is, in principle, arbitrary. So far, simple space-periodic profiles [29,30,32,33], geometric shapes with dimensions larger than the spontaneous length scales [29,36], forcing at a limited number of discrete points in the plane [24], random heterogeneities (spatial noise) [34,35,37], or even complete images [31] have been used. In this paper, we regard the spatial analog to the very first observation of temporal synchronization by Huygens. This concerned the synchronization of a periodic oscillator by a periodic rhythm; the spatial analog is the forcing of spontaneous periodic structures with static and also spatially periodic patterns.

Only recently, such a scheme has been realized in a photosensitive chemical reaction, where the synchronization of hexagonal patterns was investigated in detail [33]. In an earlier experiment on a forced polymerization reaction, already first evidence of spatial synchronization effects had been seen [32]. The use of an optical system, as presented in this paper allows one to investigate such a spatial forcing in great detail, revealing analogies to the classical synchronization of periodic oscillators.

The particular nonlinear-optical experiment we use belongs to the class of the so-called *single-feedback* systems. The system is well understood and offers a number of advantages, e.g., the clear separation of the two main ingredients for spatial instabilities: diffractional spatial coupling and nonlinearity. Because of the high sensitivity of the optical nonlinearity, it is possible to realize large aspect-ratio patterns even with low laser powers. Moreover, the dynamics of the spontaneous structure formation is determined by the comparably slow time constant of the nonlinearity. This allows us to record the complete spatial dynamics with conventional charged-coupled device (CCD) cameras.

Above a threshold of the pump intensity, hexagonal patterns form out of a stationary bifurcation [38–40]. For higher pump intensities, the patterns become increasingly disordered and dynamic [41,42]. Experimentally, these patterns are observable as intensity distribution in the cross section of a light wave.

As forcing, we use patterns of the same hexagonal symmetry and systematically change their spatial periodicity. There are two important, possibly counteracting parameters, namely, the forcing strength and the pump intensity. Increasing the first one should impose spatial order, while an increase in the second one provokes disorder. Measurements are carried out for different combinations of these parameters.

The manipulation of spontaneous optical patterns by spatially modulated forcing has been the topic of several, mostly theoretical reports [43–46]. The objectives of these authors have been different from the present paper, e.g., the selection of particular pattern states. Nevertheless, the role of the interaction of the spatial Fourier modes involved was already pointed out in Ref. [43], and first indication of spatial resonance phenomena was given in Refs. [43,45]. Experimentally, this forcing was realized by modulation of the intensity or of the phase of a light wave inside the system [46]. In our system, we will instead inject an independent, spatially modulated light wave.

The space and time dependences of the intensity distribution observed in our experiment can be rather complex. In order to receive a quantitative picture, the massive information content of recorded image sequences necessarily has to be reduced to single, characteristic measures. To date, no standard procedures have been established for such a task. We will apply and compare several characterization methods. All of them regard only the system response, i.e., do not rely on the knowledge of the actual forcing profile.

II. THE SYSTEM

A. The nonlinearity and the single feedback

The optical nonlinearity is provided by a *liquid crystal light valve* (LCLV) [47] . This multilayer device has a reflective *read* side and an intensity sensitive *write* side. The write side consists of a thin photoconductor layer and the read side is a thin liquid crystal layer. Both layers are separated by a dielectric mirror and sandwiched between two transparent electrodes to which an external, low-frequency voltage is applied. An intensity peak of the write wave causes a local decrease of the photoconductor impedance. As a consequence, the voltage across the liquid crystal layer is locally increased, leading to reorientation of the liquid crystal molecules and thus to a change of the local effective refractive index.

A read light wave passing the liquid crystal layer (and being reflected by the internal mirror) acquires a phase profile, which is determined by the intensity profile of the write wave at the other side of the LCLV. According to this intensity dependence of the phase, the LCLV provides a saturable Kerr-type nonlinearity.

The LCLV is put into an optical feedback loop. A uniform (pump) laser beam is the first phase modulated by the LCLV read side. The modulated beam is then fed back to the write side. Due to diffraction during the propagation through the feedback loop, spatial phase modulations are transformed into intensity modulations. The LCLV transforms them back into a corresponding phase profile. In such a way, the feed-

back is closed and the wave inside the feedback loop basically modulates itself.

Since the optical feedback is almost instantaneous with respect to the LCLV response time, the system dynamics is fully determined by the relaxation-type response of the LCLV, with a time constant τ in the order of tens of milliseconds. The system can be described by an equation for the phase shift $\Phi(x,y,t)$ induced by the LCLV [39],

$$\tau\dot{\Phi} - l^2\nabla_\perp^2\Phi + \Phi = S(I_w, I_f),$$

$$S = \Phi_{max}\left[1 - \tanh^2\left(\frac{1+\kappa_r(I_w+I_f)}{1+\kappa_s(I_w+I_f)}\hat{V}_{ext} - \hat{V}_{th}\right)\right] \qquad (1)$$

and by one for the intensity distribution $I_w(x,y,t)$ of the feedback wave at the LCLV write side:

$$I_w = |\exp[-i(L/2k_0)\nabla_\perp^2]\exp(-i\Phi)|^2 I_p . \qquad (2)$$

The saturation function $S(I_w, I_f)$ is determined by the LCLV parameters Φ_{max}, κ_r, κ_s, $\hat{V}_{ext}$, $\hat{V}_{th}$. Different transverse coupling mechanisms in the LCLV are approximated by a single diffusional term with an effective diffusion length $l \approx 30\ \mu$m; $\nabla_\perp^2$ being the Laplacian in the transverse coordinates x,y. Diffraction is covered by the operator $\exp(-i(L/2k_0)\nabla_\perp^2)$, with the propagation length L and the light wave number $k_0 = 2\pi/\lambda$. It can be shown that diffraction, not diffusion, is the spatial coupling mechanism responsible for the modulational instability.

By substituting Eq. (2) into Eq. (1), we can, in principle, arrive at a single partial differential equation in time and in the two transverse coordinates for a real scalar variable, the phase shift $\Phi(x,y,t)$. The model also shows that the system state is completely determined by recording the write side intensity distribution $I_w(x,y,t)$ in the experiment.

When the intensity of the pump beam I_p exceeds a certain threshold, the uniform state becomes modulationally unstable with respect to a critical transverse wave number $k_c \approx 2\pi\sqrt{3/(2\lambda L)}$ [38,39], leading to a stationary bifurcation: patterns spontaneously develop in the cross section of the feedback wave. Experimental examples are shown in Fig. 1 (as for the images in the remaining paper we use inverse gray scale, i.e., dark corresponds to large intensities). There are also higher-order critical wave numbers $k_c^{(n)} \approx \sqrt{(4n-1)/3}k_c$ present, excited at larger pump values I_p.

In Eq. 1, the forcing is represented by the intensity distribution $I_f(x,y,t)$, which is (incoherently) added to the feedback wave intensity I_w. Since the intensity distribution $I_w(x,y,t)$ is a state variable, the forcing is additive and not parametric.

The setup is called *single-feedback*, since the modulated wave is fed back to the optical nonlinearity only once, in contrast to resonators with multiple passages of the light wave. Optical resonators, moreover, impose boundary conditions on the optical field, resulting in the selection of spatial (longitudinal and transverse) modes. Diffractional losses and possibly a wavelength dependence of the optical nonlinearity lead to an additional favoring of particular modes. Conversely, a corresponding preselection of spatial profiles does not exist in single-feedback systems.

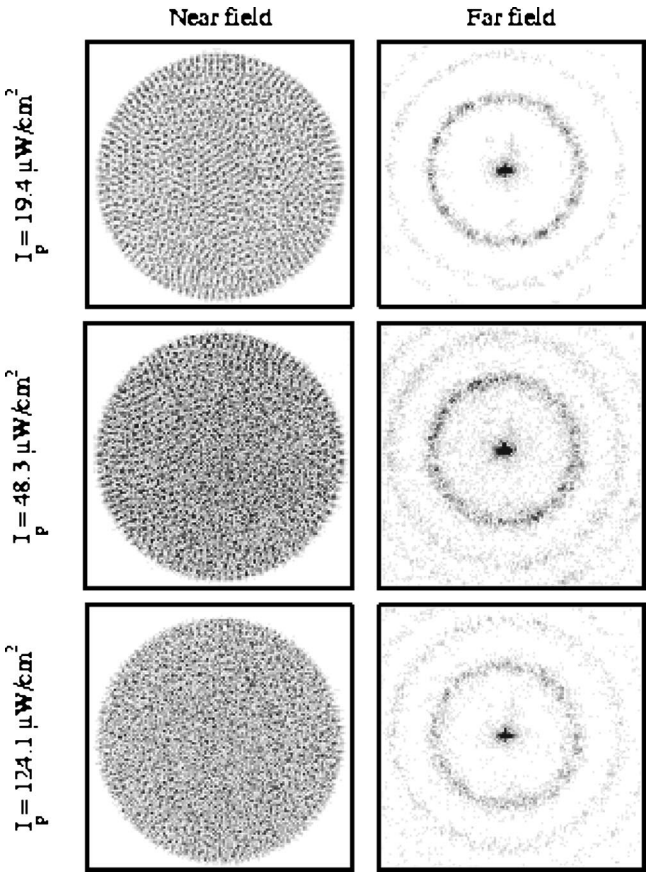

FIG. 1. Autonomous, unforced system at the different levels of pump intensity (as indicated). From top to bottom: just above pattern forming threshold, at 2.5 times and at 7 times threshold. Left-hand side, optical near field $I_w(x,y)$; right-hand side, optical far field.

The class of single-feedback systems has become quite popular in the last years [38,39,48,49]. The use of LCLVs as optical nonlinearity, first introduced by Akhmanov, Vorontsov *et al.*, has proven to offer a great experimental flexibility in various implementations. In several variants, a rotation [50,51] or a lateral shift [52] of the feedback wave was introduced to provide a nonlocal spatial coupling. Such geometrical transformations break the continuous symmetry by distinguishing a particular angle and/or length scale. In contrast, we use the fully symmetric system with diffraction as a global spatial coupling mechanism [53], in correspondence with the original single-feedback scheme proposed in Ref. [38]. Concerning the nonlinearity, it is possible to introduce an additional dependence of the feedback intensity on the phase, e.g., with a resonator or a polarizer. This alters significantly the underlying nonlinearity and hence affects the observable spontaneous patterns [39,54]. In the system used here, the nonlinearity is of saturable Kerr type with a monotonous intensity dependence of the induced phase.

B. Experimental setup

The experimental setup is shown in detail in Fig. 2. As a light source, a frequency doubled Nd:YAG (yttrium alumi-

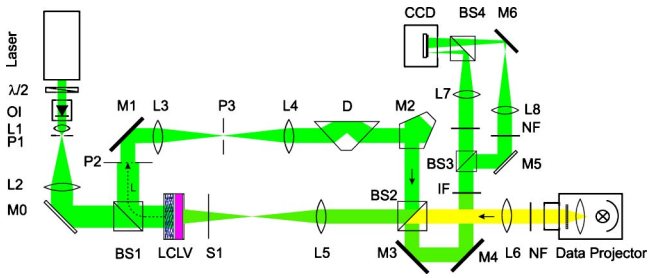

FIG. 2. Experimental setup. For details, please refer to the text.

num garnet) laser ($\lambda = 532$ nm) is used. The light power is regulated by a rotatable half-wave plate ($\lambda/2$), acting together with the internal polarizers of the optical isolator (OI). The beam is cleaned and expanded to a diameter of around 5 cm by the 4-f-arrangement L1, P1, L2. This pump beam enters the setup via the beam splitter BS1.

The pump wave is reflected and phase modulated by the LCLV read side (liquid crystal layer) and then fed back to the LCLV write side (photoconductor layer) by means of beam splitters BS1 and BS2, a mirror M1, and a penta prism M2. During feedback, the modulated beam propagates freely over a distance $L = 200$ mm to the plane of aperture P2. The wave front in this plane is imaged by the lenses L3, L4, L5 to the LCLV write side. The aperture P2 (diameter $D = 8.5$ mm) cuts out the active area.

A rotatable dove prism D is used to correct residual rotations of the feedback wave around the optical axis, which may occur through slight misalignments of the mirrors. A shutter S1 in front of the LCLV write side can cut off the feedback wave and the forcing simultaneously. In the Fourier plane between L3 and L4, an aperture P3 can be used to low-pass filter the wave, which is, however, not used in the present experiments.

For detection purposes, part of the feedback wave leaves the setup through BS2. The forcing wave, which also leaves the setup here can be blocked by an interference band pass filter IF, which transmits the laser wavelength only. Hence, in effect only the feedback wave is detected by the CCD camera. The detection path is split into two arms in such a way that both the near field, i.e., an intensity distribution corresponding to the one at the LCLV write side, as well as the optical far field in the focal plane of lens L7, i.e., the spatial power spectrum of the feedback wave, are recorded simultaneously.

We use a 12-bit digital CCD camera (PCO SensiCam) with a resolution of 640×480 pixel. Movies of up to 331 images are directly transferred to the random access memory of the connected PC. In the present case, we used frame rates of around 7 frames per second. A conventional power meter was used to control the optical power in front of the LCLV write side, of both the feedback wave and the forcing wave. The readings for white light forcing wave were scaled to illuminance units.

The LCLV is manufactured by Jenoptik LOS GmbH, Jena. We operate the LCLV with an external voltage of $2.5V_{pp}$ at 170 Hz (sine wave). The photoconductor is amorphous silicon (thickness 3 μm) and the nematic liquid crystal is a conventional mixture for displays (TN0304 by Merck, thickness 6 μm).

For the particular parameter settings, ideal hexagons are hard to realize experimentally. Instead, we see only small hexagonal domains or even domains with quasicrystalline character (which were not observed in previous experiments with a smaller aspect ratio). However, even disordered spontaneous patterns contain only the critical Fourier modes, i.e., the corresponding far field consists of broadly excited rings (cf. Fig. 1). By applying an experimental control technique, we have recently proven that hexagons are indeed a stationary system state, at least up to two times threshold [40,55]. This corresponds to a theoretical analysis of a similar system [38]. Consequently, by using hexagons, the system will be forced with one of its own (unstable) states—or at least a very similar one when the forcing wave number is altered.

It is possible to simplify the system by cutting off the higher-order critical wave numbers with the spatial low pass filter (L3, L4, and P3). In this case, almost perfect hexagons can be found up to several times threshold [41,42]. However, filtering also inhibits forcing with wave numbers $k_f > k_c$. Moreover, the interaction via spatial harmonics would be blocked. Hence, in contrast to our previous experiment [56], low pass filtering is not applied.

Another disturbance of perfect patterns results from small inhomogeneities of the LCLV, caused by smooth variations in the thickness of the photoconductor layer. As a consequence, the pattern formation threshold slightly varies across the transverse plane. In order to achieve the best possible uniformity, only a small active area is cut out by the aperture P2. We must also consider that—at least for the autonomous system—the presence of boundaries causes the pattern to grow smoothly from the center [40]. Consequently, there is no sharp threshold, we will here refer to an average value of $I_{th} \approx 18.8\ \mu\mathrm{W/cm}^2$.

C. Forcing

The write side of the LCLV has a broad spectral sensitivity, which allows us to use incoherent light for the forcing. This will avoid interference between the forcing and the feedback wave and the connected sensitivity to vibrations.

To generate almost arbitrary forcing patterns, we used a data projector, containing a conventional halogen bulb as a light source and a transmissive liquid crystal display (LCD). The display was imaged onto the LCLV write side by the lenses L5, L6. The projector intensity was attenuated by a fixed set of neutral density filters (NF). Each of the 832×624 LCD pixels can take 254 gray levels. Due to a software controlled linearization, the gray levels correspond to a linear change in transmitted light intensity. The projector has an internal memory for 31 images, which are loaded by a serial interface. Since the measurements were carried out with 59 different forcing patterns, each measurement had to be interrupted once for about 25 min for loading a new set of images.

The projector illumination is not completely homogeneous across the area of the display, with a maximum inten-

sity variation of $\pm 30\%$. This smooth inhomogeneity was compensated by using the inverted illumination profile as an envelope of the forcing pattern. Due to this superimposed modulation amplitude, the remaining modulation depth usable for the forcing profile is reduced.

The operating point of the LCLV is shifted towards saturation by the additional illumination [cf. Eq.(1)]. Thus, the average of the forcing intensity had to be kept constant throughout all measurements. The modulation amplitude A_f of the forcing profile was controlled by the gray levels of the projector LCD only.

Before turning to the measurements, we briefly have to discuss the spatial harmonics, appearing due to the forcing. Even without interaction with the spontaneously forming pattern, the forcing intensity distribution $I_f(x,y)$ induces a corresponding phase profile in the pump wave $E_p \sim \exp[-i\Phi] \sim \exp[-iS(I_f(x,y))]$ [cf. Eqs. (1) and (2)]. Since the forcing pattern consists of few discrete modes $\vec{k}_{fj}$ only, this nonlinearity causes—depending on the amplitude of the intensity pattern—the appearance of a number of harmonics. In Fourier space, i.e., in the far field, these spatial harmonics simply are linear combinations of the fundamental wave vectors $\vec{k}_{fj}$.

The modulus of a resulting harmonic[1] mode can be an integer multiple of the fundamental wave number (''straight'' harmonic), but can also be an irrational multiple, when the harmonic mode is a noncollinear combination of different fundamental wave vectors (''mixed'' harmonic). Hence, irrational multiples of fundamental wave numbers naturally emerge in two dimensions. In the following, most important are the mixed harmonics with modulus $\sqrt{3}k_f$ and $\sqrt{7}k_f$.

The resolution of all modes in the system is limited by the aspect ratio. Due to the finite diameter D of the active area, each mode is broadened to a width $\Delta k \approx 2\pi/D$. For the spontaneous patterns, we have an aspect ratio of 33, i.e., a broadening of the modes of about 3%. For the smallest forcing wave numbers, this broadening can reach 10%.

D. The measurements

Forcing is investigated under systematic change of the wave number k_f of the forcing pattern. Parameters for each such a measurement are the forcing amplitude A_f and the pump intensity I_p. As forcing, we choose peak-to-peak amplitudes of the hexagonal patterns of 10, 35 and 138 LCD gray levels with a constant offset at gray level 71. The pump was set to values just above threshold, to 2.5 times threshold and to 7 times threshold. During each measurement, the pump intensity was checked to be constant within $\pm 3\%$. With these settings, eight measurements were carried out in the parameter field (A_f, I_p), as schematically depicted in Fig. 3. We renounced on a measurement with low forcing amplitude and large pump intensity, since it appeared that forcing would have no effect.

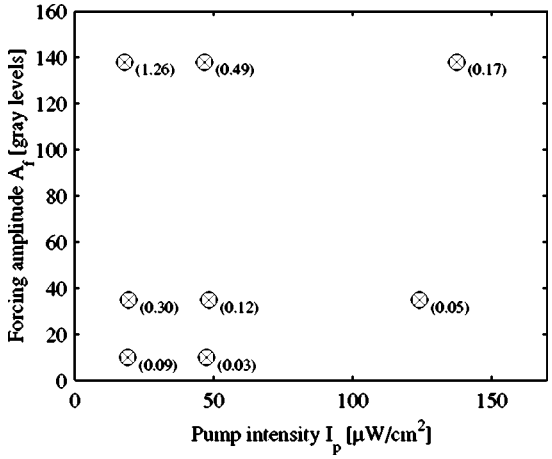

FIG. 3. Location of the measurements in the parameter field forcing amplitude A_f and pump intensity I_p. The numbers in brackets denote the estimated relative forcing strength, as discussed in Sec. II E.

For each fixed set of the parameters (A_f, I_p), measurements were carried out under systematic variation of the forcing wave number k_f. The upper limit of k_f was given by the spatial resolution of the LCD in the data projector. We used a minimum wavelength of 6 pixels and a maximum wavelength of 60 pixels. This resulted in a range of $0.275 \leqslant k_f/k_c \leqslant 2.75$, covered with 59 sample points.

For each fixed forcing pattern, the system was switched on by opening the shutter S1 in front of the LCLV write side. In such a way, the system itself is switched on simultaneously with the forcing. We have found in other experiments that this choice results in considerably shorter transients than for the case that the system is switched on first and the forcing has to reorder an already existing structure [57]. Just before opening the shutter, the camera was started, recording a sequence of 331 images with a duration of around 45 s. The measurement for a specific parameter set (A_f, I_p) took about one day. All measurements together correspond to around 100 Gb of raw image data, which makes it necessary to apply a computer based analysis to identify particular interesting system responses.

After each recording, the pump wave was blocked and the LCLV was ''blinded'' for a short period by an intense white light to erase any possible residual memory of the last pattern state. During the variation of the forcing pattern, a number of measurements of the autonomous, i.e., unforced system were carried out, referred to as *reference measurements* in the following. For this means, the LCD was set to the uniform offset level.

As already mentioned, each measurement had to be interrupted once for about half an hour, to load the projector with a new set of images. Also, the forcing wave number was not changed monotonously. Starting at large values, k_f was systematically decreased, but a number of intermediate large values were recorded later. The analysis of the recorded data revealed that the system appeared to have drifted slightly during the measurement. The reordering of the sample points seemingly leads to jumps in some of the extracted quantitative measures. All of the measures derived below were cor-

[1]Sometimes the term ''harmonic'' is used for the fundamental modes themselves, while instead here, we use it for linear combinations of those.

rected with the help of the reference measurements. However, due to the limited number of reference measurements, complete correction was not possible.

The drift was presumably caused by changes in the lab temperature—the LCLV is qualitatively known to be somewhat temperature sensitive. Depending on the particular measurement, the temperature change could reach $\Delta T = 2$ K during the day and less than 4 K between different days.

E. Forcing strength

A statement of the forcing strength, i.e., the amplitude of the forcing intensity modulation, makes only sense when compared to the amplitude of the spontaneous patterns. The forcing pattern itself is well defined, consisting of three pairs of conjugated Fourier modes with given amplitudes. In contrast, the spontaneous system state, particularly further above threshold, is determined by the excitation of one or more critical rings in Fourier space. We have found the standard deviation σ_w of the near field intensity distribution I_w to be a suitable measure to compare the spontaneous excitation to the imposed one:

$$\sigma_w = \sqrt{\frac{1}{N-1}\sum_{j=1}^{N}(I_{wj}-\langle I_w\rangle)^2}. \tag{3}$$

Here, I_{wj} is the intensity at pixel number j of the CCD camera, $\langle I_w\rangle$ is the average value, and the sum goes over all N pixels. We have found that, in particular, the relative standard deviation of the spontaneous patterns does not depend very much on the pump intensity $\sigma_w/I_p \approx 0.781 \pm 3\,\%$.

In a separate measurement, the white forcing light is compared to the monochromatic feedback wave by measuring the phase shift induced in the LCLV. An illuminance of 7.02 lx induces the same phase shift Φ as a monochromatic write intensity of 1 μW/cm^2. Together with the dependence of $\Delta I_f = 0.449$ lx per LCD gray level, and the standard deviation of an ideal hexagon, we arrive at a corresponding relative standard deviation of the forcing patterns of $\sigma_f/A_f = 0.1286\,\mu\mathrm{W}/(\mathrm{cm}^2)$ per gray level.

In Fig. 3, the ratios σ_f/σ_w between both standard deviations are given in brackets as an estimation of the relative forcing strength. Within this definition, our measurements vary between weak forcing of some few percent and strong forcing, where the forcing amplitude is in the order of the spontaneous excitation.

III. RESULTS

A. Synchronization

Under variation of the forcing wave number, we observe an almost binary response of the system. Either, it completely locks onto the forcing, which means that the system state becomes steady state and has a similar spatial structure and the same orientation as the forcing pattern. Otherwise, the system reacts with pronounced spatiotemporal disorder.

A first impression can be gained from the snapshots presented in Fig. 4. Clearly, the system is entrained when the forcing wave number equals the basic critical wave number $k_f = k_c$. In order to achieve a more quantitative picture, it is necessary to extract adequate measures from the often complex system response. Here, we renounce on computing the cross correlation between forcing patterns and system response, since this would not cover possible spatial phase shifts between both.

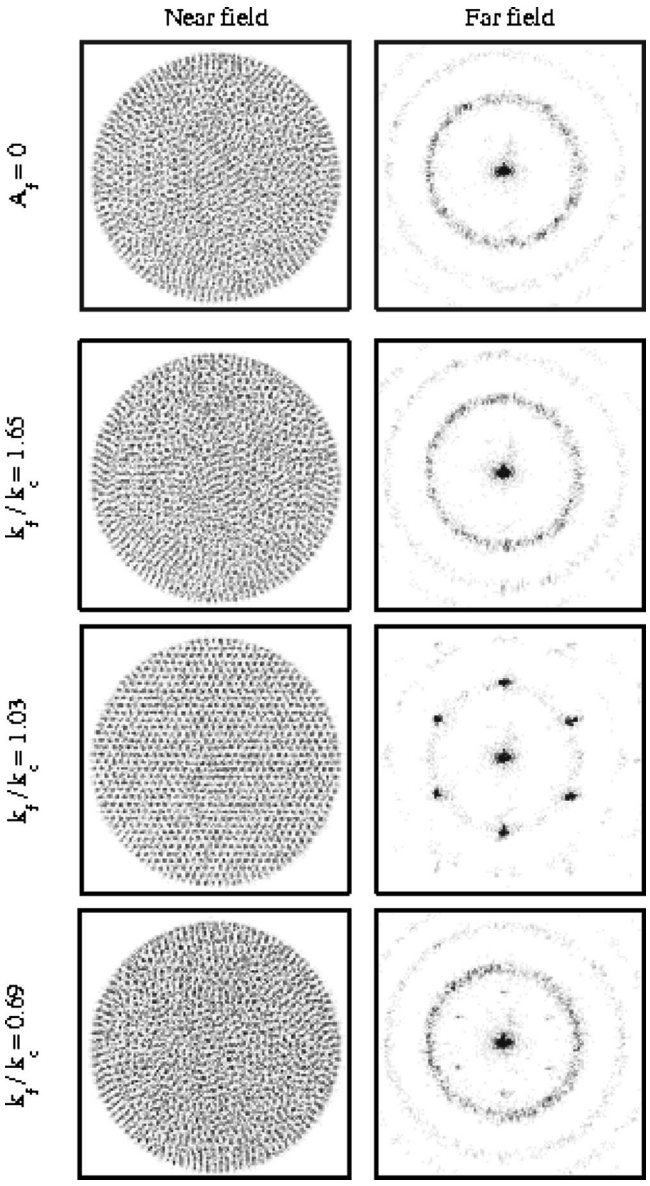

FIG. 4. Examples of snapshots of the system response to hexagonal forcing at different wave numbers (as indicated). The images are presented in inverse gray scale (dark = large intensity). For comparison, the top patterns present the unforced system. In this example, the pump intensity just above threshold and a moderate forcing amplitude is applied ($A_f = 35$). Presented are the near fields (lhs column) and the far fields (rhs).

B. Wave number spectrum

The recorded far field gives valuable information about which wave numbers are excited. For this means, the far field

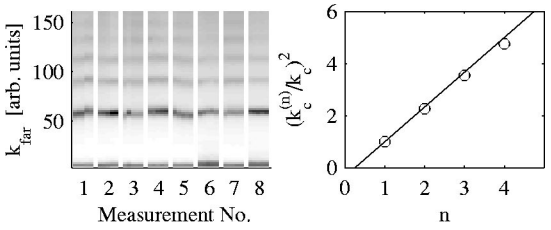

FIG. 5. Left-hand side: identification of the critical wave numbers from the reference measurements. Right-hand side: check of the approximate relation between the different order critical wave numbers.

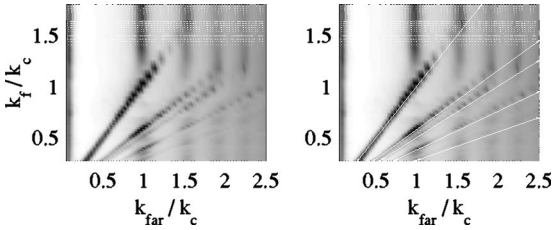

FIG. 7. Wave number spectrum for large forcing amplitude and medium pump intensity. In the rhs panel, straight lines are added, denoting the expected slopes for different harmonics of the forcing wave number.

intensity distribution $I_{\mathrm{far}}(\vec{k})$ is integrated over the angle, thus reducing the two-dimensional wave *vector* spectrum to a one-dimensional wave *number* spectrum I_k.

The wave number spectrum is first computed for the reference measurements to identify the spontaneously excited wave numbers. In Fig. 5, the basic critical wave number $k_c = k_c^{(1)}$ and at least three higher-order critical wave numbers $k_c^{(n)}$ are clearly identifiable. These do not change considerably between the measurements. The resulting values of $k_c^{(n)}$ have an error of $\pm 3\%$, which is around twice the resolution of this evaluation, limited by the pixel size of the CCD camera. The approximative relation between the different critical wave numbers $k_c^{(n)} \approx \sqrt{((4n-1)/3)}k_c$ [38] is plotted for comparison (right-hand side of Fig. 5).

In Fig. 6, I_k is shown for the forcing measurements. The individual plots are schematically arranged according to the location of the parameter pair (A_f, I_p) in the parameter plane, as depicted in Fig. 3; the pump intensity increases from left- to right-hand side, the forcing strength increases from bottom to top. In each individual graph, the abscissa represents the scaled wave number k_{far} of the far field, the ordinate is the scaled forcing wave number k_f and I_k is shown in inverted gray scale. The pronounced vertical lines correspond to the different critical wave numbers $k_c^{(n)}$, which are almost always excited. The excitation induced by the forcing is reflected in different oblique straight lines, belonging to the forcing wave number $k_{\mathrm{far}} \sim k_f$ and the different harmonics of the forcing modes. As expected, the effect of forcing is found to be most pronounced for large forcing strength and low pump power.

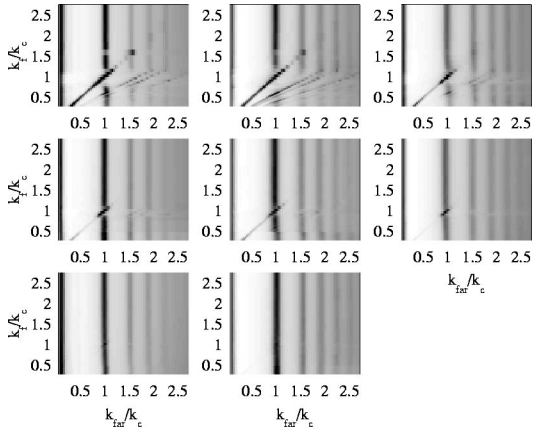

FIG. 6. Wave number spectra (in inverse gray scale) as a function of far field wave number k_{far} and forcing wave number k_f. The plots are arranged according to the values of the parameter pair (A_f, I_p): the forcing strength increases from bottom to top, the pump intensity from left- to right-hand side.

Figure 7 shows a particular measurement in more detail. The added straight lines correspond to slopes of $k_f/k_{\mathrm{far}} = 1$, $1/\sqrt{3}$, 1/2, $1/\sqrt{7}$, and $1/\sqrt{13}$, verifying that all these harmonics are indeed excited. Diffusion damps higher wave numbers, which explains the lower excitation of higher harmonics. The third straight harmonic wave number $3k_f$ is not even visible anymore, while the $\sqrt{7}$ mixed harmonic still is present, because 12 instead of just 6 modes have this modulus. Close to the $\sqrt{13}$ harmonic, the $2\sqrt{3}$ harmonic exists. Together, these represent 18 modes, which in the same manner balances the diffusional damping.

Two important findings can be taken from Fig. 6. First, if the system locks onto a particular forcing wave number, power is even drawn out of other critical wave numbers. This is most prominent for $k_f = k_c^{(2)} \approx 1.5k_c$ (for strong forcing, small or medium pump power), when even the excitation of the fundamental critical wave number is reduced.

Second, we find a ''mode pulling'' effect, when the forcing wave number k_f comes close to one of the critical wave numbers $k_c^{(n)}$. In the wave number spectrum, this corresponds to the vicinity of a crossing between an oblique and a vertical line. Here, the excitation completely migrates from the critical wave number into the forcing wave number.

C. Spectral localization

There is a rather simple method to characterize the degree of spatial order by utilizing the far field. For periodically patterns, the total power in the far field is distributed among few, localized modes, while the spatial disorder corresponds to broadly excited areas. Consequently, localized modes correspond to large values appearing in the frequency distribution of the far field intensities, while in the disordered case the maximum intensity will be considerably lower. The majority of the amplitudes will, however, always be zero or very small.

Nevertheless, with the standard deviation of the far field intensity distribution σ_{far}, the presence of localized modes can be detected. In this analysis, the zero order was cut out, since it is always localized, carrying the largest amplitude in the far field. Deleting the zero order makes also sense in the

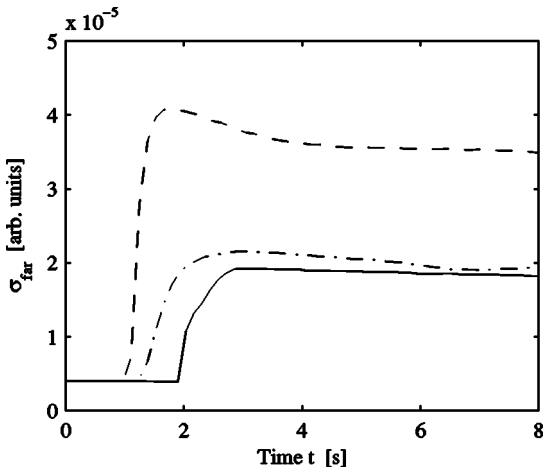

FIG. 8. Typical temporal evolution of the far field standard deviation for $k_f/k_c=1.03$ (solid line), $=1.61$ (dashed line), and $=2.64$ (dash-dotted line). The pump intensity is set just above threshold and the forcing amplitude is medium ($A_f=35$).

respect that we are only interested in spatial modulations.

The computation of the far field standard deviation σ_{far} allows us to follow the dynamics of the forced patterns. The temporal evolution of $\sigma_{\mathrm{far}}(t)$, presented in Fig. 8, shows that the transients are rather short. After typically less than 2 s, the system is in its asymptotical state. Only close to pronounced locking regimes, the transient can take longer, but never more than few seconds. Hence, the largest part of the recorded system response corresponds to the statistically stationary state.

The standard deviation σ_{far} was computed for a representative number of images from each sequence and averaged. The result for all forcing measurements is plotted over the scaled forcing wave number in Fig. 9. The horizontal lines

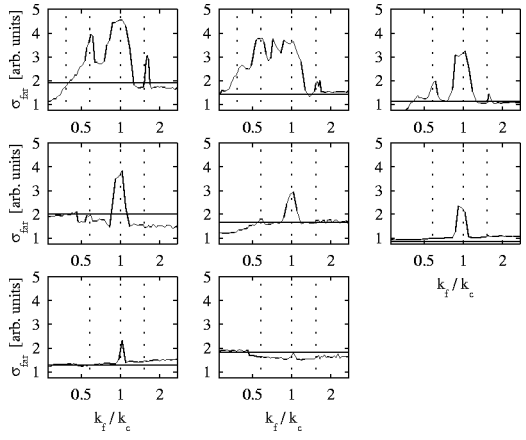

FIG. 9. Standard deviation of far field intensities σ_{far} (in arbitrary units) plotted against the scaled forcing wave number (in logarithmic scale). The plots are arranged schematically in parameter plane according to the values of A_f (increasing from bottom to top) and I_p (increasing from left- to right-hand side). The horizontal lines correspond to the unforced system, the vertical, dotted lines indicate expected resonances at $k_f=k_c$, $\sqrt{3}k_f=k_c$, $k_f=k_c^{(2)}$, and for strong forcing also at $\sqrt{7}k_f=k_c$.

represent the average values of the reference measurements of the unforced systems. The dependence of these reference values on the pump intensity reflects the general tendency of a decreasing spatial order with an increasing pump strength.

The important point here is the appearance of a number of peaks. These indicate different locking regimes, where the system response collapses from a broad spectral excitation to few modes. Again, we find that the effect of forcing increases with forcing amplitude (from bottom to top in Fig. 9) and, in general, becomes weaker with increasing pump power (from left- to right-hand side in Fig. 9). In particular, the peaks become more pronounced and wider with increasing forcing strength. This phenomenon appears to be a spatial analogy to the Arnold tongues [1].

The most prominent peak, which is present in almost every measurement, belongs to the locking of the forcing wave number onto the fundamental critical wave number $k_f=k_c$. The other peaks belong either to a locking of a harmonic of the forcing pattern onto k_c or to a locking of the forcing onto a higher critical wave number. In particular, we find the mixed forcing harmonics $\sqrt{3}k_f$ and $\sqrt{7}k_f$ to lock onto k_c. Also, the entrainment of $k_f=k_c^{(2)}$ is observed. By chance, the locking at $\sqrt{3}k_f=k_c$ coincides with a locking of another forcing harmonic on the second critical wave number $\sqrt{7}k_f=k_c^{(2)}=\sqrt{7/3}k_c$. Dashed vertical lines in Fig. 9 indicate these ratios between $k_c^{(n)}$ and k_f. We see so far no indication of locking at integer ratios $k_f=2k_c$ or $2k_f=k_c$, even though this second harmonic of the forcing has already been identified to be excited in Fig. 6.

The different locking constellations are demonstrated in Fig. 10, where the near field and the far field of the system response are shown. From the location of the modes in the far field, the described relations between forcing modes and critical wave numbers can easily be verified. We note that some near field patterns in Fig. 10 are less ordered in the lower central part. We assign this to the influence of the remaining inhomogeneity of the LCLV. For the small forcing wave number at $k_f=k_c/\sqrt{7}$, we observe small bright spots ordered around darker and larger ones. The size of the small spots corresponds to the spontaneous patterns. The larger spots result from the fact that we have a defocussing nonlinearity. In a very simple picture, each (large) spot of the forcing pattern can be imagined to induce a defocussing lens in the LCLV read side, i.e., the pump intensity is refracted out of these areas.

So far, the quantitative analysis of the far field does not yield information about the (rotational) symmetry of the evolving patterns. Also, not much can be deduced about a possible dynamics of the system state, either due to intramode dynamics or due to any dynamics hidden in the phases of the modes—such as in the case of moving patterns or waves.

D. Characterization of the dynamics

Rather the opposite approach to characterize the system response is to consider the dynamics only, completely ignoring any spatial order. For this means, we compute the autocorrelation of the local temporal evolution of the near field.

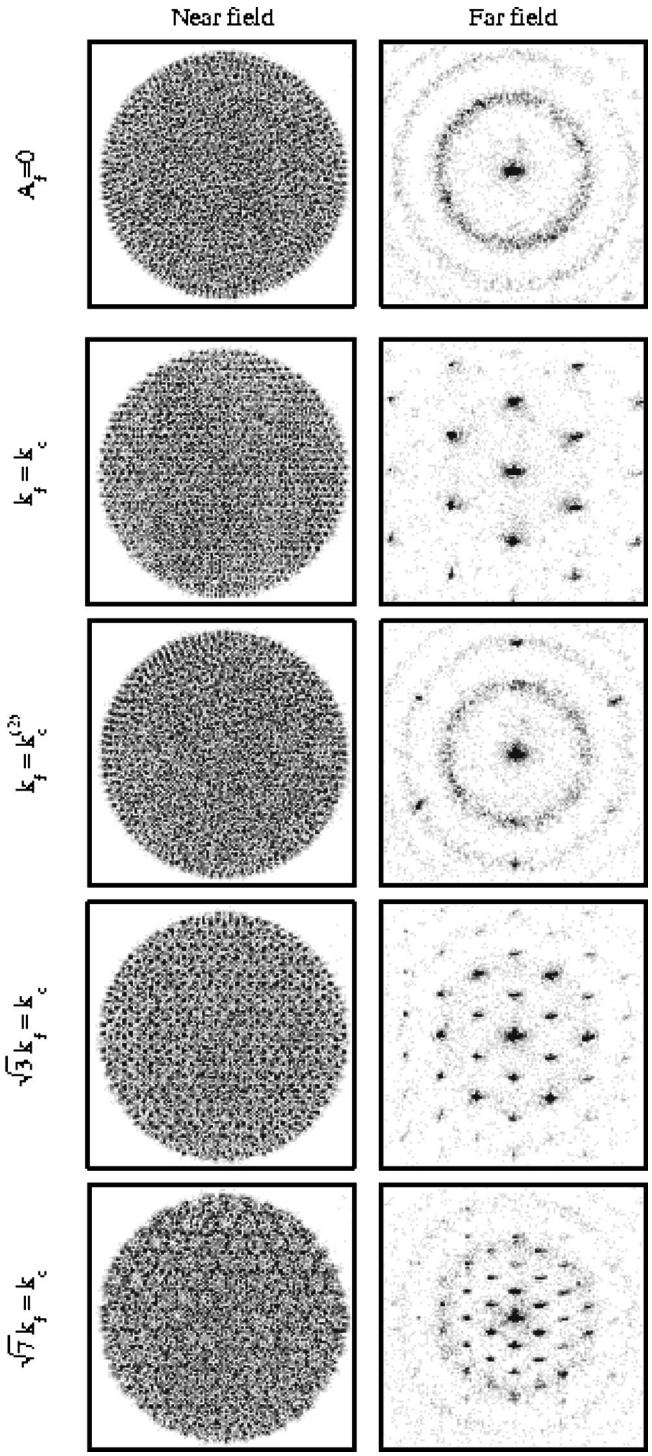

FIG. 10. System response in the unforced case (top), compared to typical locking constellations, as indicated. The pump intensity is 2.5 times threshold, forcing is strong.

Included are only the last two-third of every recorded sequence, in order to be sure to omit the transients. The autocorrelation is averaged in space as

$$\langle K(\Delta t)\rangle_{x,y}=\int \hat{I}_w(x,y,t-\Delta t)\hat{I}_w(x,y,t)dt\,dx\,dy. \quad (4)$$

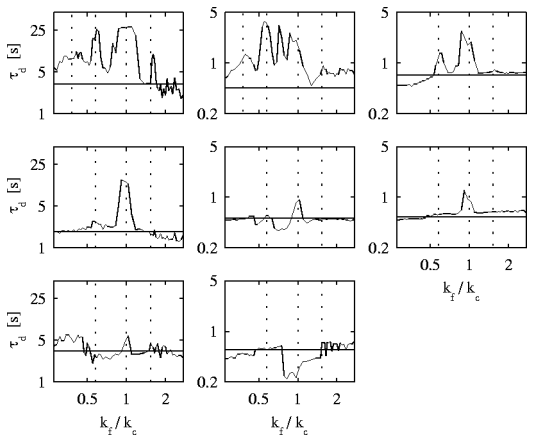

FIG. 11. Time constants characterizing the near field dynamics plotted against the scaled forcing wave number, in double logarithmic scale. Note the different scales for τ_d. The plots are arranged schematically in parameter plane according to the values of A_f (increasing from bottom to top) and I_p (increasing from left to right-hand side).

Here, $\hat{I}_w(x,y,t)=I_w-\langle I_w\rangle$ is the recorded intensity sequence $I_w(x,y,t)$, subtracted by its average $\langle I_w\rangle$.

From the spatially averaged autocorrelation function, we can extract a typical time constant τ_d by fitting an exponential function into the first decay. The fit interval is adapted to the steepness of the decay. A large value of τ_d corresponds to slow dynamics or even a static pattern. The maximum detectable value of τ_d is limited to around 30 s, which is the duration of the analyzed sequences.

Figure 11 presents the time constants for all measurements, plotted over the scaled forcing wave number. We again find the typical peak structure, indicating the different locking regimes. Obviously, in the case of locking, the static forcing patterns ideally cause a static system response. The underlying tendency of the unforced system to build up a turbulent state leads to a residual dynamics. As a consequence, the observed time constants decrease with increasing pump power.

In comparison with the results of the preceeding section, we here see a more pronounce locking, i.e., a peak of larger time constant, at low forcing wave number, high forcing amplitude, and low and medium pump intensity. The rather broad peak probably contains a resonance at $\sqrt{7}k_f=k_c$, marked by vertical lines.

We also note a rather fluctuating background for $\tau_d(k_f)$, in particular, for the case of weak forcing and medium pump intensity. Part of these fluctuations, in particular, the jump at $k_f/k_c\approx 0.75$ and the smaller dips at $k_f/k_c>1.4$ are caused by the above mentioned drift and the reordering of the sample points. Moreover, the time constants found for the reference measurements vary between the different parameter sets. This is the consequence both of the drift and of the general dependence of the time constant on the pump intensity [41].

E. Degree of spatial symmetry

Finally, we characterize the degree of spatial order by quantifying the degree of hexagonal symmetry [58]. We

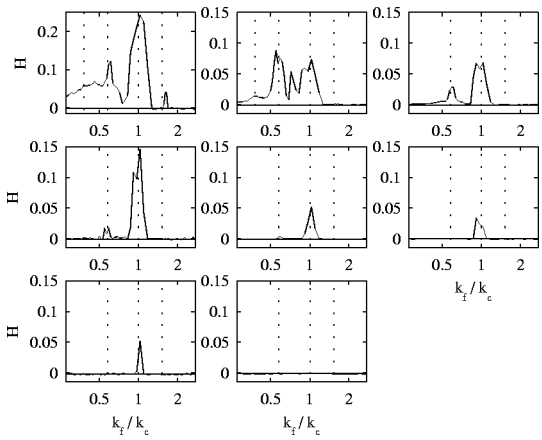

FIG. 12. Hexagonal symmetry parameter H, characterizing the average degree of sixfold symmetry, plotted over the scaled forcing wave number (in logarithmic scale) for all measurements. The plots are arranged schematically in parameter plane according to the values of A_f (increasing from bottom to top) and I_p (increasing from left- to right-hand side).

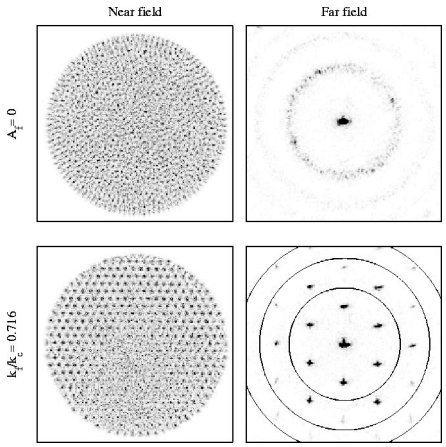

FIG. 13. Comparison of unforced system response (upper panels) with the one for locking at $k_f=0.716\,k_c$ (lower panels) at strong forcing and medium pump. For better visualization, the critical wave number circles have been added.

again use autocorrelation functions, now correlating an individual snapshot to its rotated counterpart.

$$C(\theta,x_0,y_0)=\int |\hat{I}_w(x,y)\hat{I}_w(x',y')|dx\,dy, \qquad (5)$$

x',y' being the rotated coordinates and θ the rotation angle. This is done for many rotation centers (x_0,y_0), over which we average $C(\theta,x_0,y_0)\rightarrow\langle C(\theta)\rangle_{x0,y0}$. The resulting average rotational autocorrelation function will peak at angles of $\theta=2\pi/N$, when the analyzed structure contains an N-fold rotational symmetry. Assuming that only a limited number of discrete rotational symmetries are present, the contributions to the different peak amplitudes can be decomposed [58]. This yields several symmetry parameters, measuring the presence of roll-, square-, or hexagon-patterns. Moreover, quasipattern symmetries can be detected. We will here use only the measure for the hexagonal symmetry $H=\frac{1}{2}[\langle C(\theta=60°)\rangle+\langle C(\theta=300°)\rangle]-O$, where O stands for a constant offset corresponding to a continuous symmetry, e.g., caused by the spatial noise.

From the present analysis, we find—with one exception—no presence of other rotational symmetries, neither tiling patterns ($N=2$, 3,4) nor quasipatterns ($N=8$, 12). The exception is a small contribution of twofold symmetry at $k_f=k_c^{(2)}$, for large forcing amplitude and low and medium pump power. In these particular cases, we also find that two of the six modes on the second critical circle are stronger excited than the others. For this finding, we do not have an explanation so far.

The average of the hexagonal symmetry parameter H found for a representative number of images of each sequence is plotted in Fig. 12 over the forcing wave number. This symmetry analysis gives the clearest peak structure. Again, we find the same locking regimes as before, which means that locking is always connected to a hexagonal system response. Compared to the analysis of the dynamics, the fluctuations in the plots of $H(k_f)$ are considerably smaller. This indicates that the above mentioned influence of temperature drifts mainly affects the LCLV time constant τ.

The main peak at $k_f=k_c$ seems to have a double peak structure, at least for stronger forcing. This results possibly from a resonance at $\sqrt{3}k_f=k_c^{(2)}\Rightarrow k_f/k_c=0.882$. This assumption is supported by the corresponding wave number spectrum in Fig. 6.

For strong forcing and medium pump intensity, an extra peak is observable between the $k_f/k_c=\sqrt{3}$ and the $k_f/k_c=1$ locking regimes, with its peak value at $k_f/k_c=0.723$. The corresponding patterns are shown in Fig. 13. In fact, this peak would be compatible with a resonance of the $\sqrt{7}$ harmonic of the forcing on the third critical wave number at $k_c^{(3)}=\sqrt{11/3}k_c$. However, these wave numbers are all quite large and strongly damped. It does not seem very reasonable that these should induce such a pronounced locking.

There is an alternative, although purely empirical explanation, which also yields a good quantitative correspondence [59]: The rational winding numbers of nonlinear resonances in oscillators can be found from the Farey construction [60–62]. A particular m:n resonance has two ''parent'' resonances at ratios p:q and r:s between the forcing and the natural frequency. The resulting winding number is found by adding nominators and denominators separately $m=p+r$, $n=q+s$. To receive the full Farey tree, one has to start with the ratios 0:1 and 1:1 and to carry on with all possible combinations. Devil's staircase, which is well known to contain all winding numbers of particular nonlinear oscillators, is just one branch of the Farey tree.

In our case, the peak in question is the ''child'' of the adjacent resonances, resulting in an expected winding number of $(1+1)/(1+\sqrt{3})\approx 0.732$, which is in good agreement with the experimental value. Higher-order children resonances are less excited and therefore here we see only the child of the two dominant basic resonances.

The application of this scheme can also reproduce the absence of simple 1:2, 1:3, 2:3, etc., resonances. Following the Farey construction, these rational winding numbers are

all based on the presence of the fundamental 0:1 winding number. However, such a 0:1 ''resonance'' does not appear in our system; a spatially uniform forcing ($k_f=0$) leads to a constant phase shift of the read wave, which does not affect the write side intensity distribution. Hence, the system does not respond to a uniform forcing—at least as long as saturation effects due to strong forcing are negligible.

In a previous publication [15], a spatial period tripling had also explicitly been predicted for forcing a two-dimensional system with hexagonal patterns and has not been found here. The system considered there was assumed to exhibit a spatiotemporal Hopf bifurcation, which is in contrast to the optical system investigated here.

For one-dimensional systems, the analysis of theoretical models had lead to the prediction of quasipatterns [9], which are also not observed in our experiment. This may be connected to the difference in dimensionality of the systems. The questions of forcing induced defects, which had also been found in one-dimensional models, is still open. The image data, gathered in our experiment, have not yet been analyzed in this respect.

IV. CONCLUSION

We have presented experimental results on spatially periodic forcing of a nonlinear optical, pattern forming system. Forcing was carried out under a systematical variation of the forcing wave number and for different values of forcing strength (between several and about 100% of the natural pattern amplitude), and also for different values of the control parameter, the pump intensity.

We found that the spontaneous optical structures can be entrained by an external forcing with static patterns. The entrainment can even be observed far above threshold of pattern formation. A number of different locking regimes were found, which are mostly caused by a resonance of the forcing wave number or one of its spatial harmonics with the fundamental or the first higher-order critical wave number. In contrast to one-dimensional systems, irrational multiples of the fundamental wave number generically appear as spatial harmonics. The width of the observed locking regimes increases with forcing strength, which is in obvious analogy to the Arnold tongues in one-dimensional systems.

One of the observed locking regimes can successfully be explained by an extension of the Farey construction, which is used to derive the rational winding numbers in a purely temporal synchronization. The connection to the Farey scheme, which does not explain the underlying physical mechanisms, is only empirical and certainly needs verification in other systems.

The role of the control parameter appears to be in general to counteract the forcing: with increasing pump intensity, the locking regimes become fewer and smaller. This corresponds well to the role of the control parameter in the unforced system, namely, to promote disorder with increasing distance from threshold.

The system response has been quantitatively characterized with respect to the spectral localization (presence of localized Fourier modes), the dynamics and the rotational symmetry. All measures give very similar results, from which we conclude that the system response in the case of locking always is a static hexagonal pattern and a very disordered and dynamic state otherwise. The analysis of the far field also revealed that, in the case of locking, spectral power is concentrated on the excited (forcing) mode, draining power also from other critical wave numbers.

In a conceptually similar investigation of forcing of a reaction-diffusion system, Dolnik *et al.* also observed some regimes of entrainment, however, at different forcing wave numbers. So far, it is not clear that whether these differences are due to differences in the underlying systems, in the experimental procedure or in the data analyses.

Our findings indicate that in two-dimensional systems, a wealth of resonances can appear. Besides the various resonances between the different order critical wave numbers and the forcing and its spatial harmonics, resulting children resonances may be expected. Even though the aspect ratio achieved here is rather high—at least for optical pattern formation experiments—the wave number definition is limited by the aspect ratio. This possibly promotes a merging of different locking regimes. For a more precise determination of locking regimes, this restriction has to be overcome independently of the type of system.

The presented experiment has shown that an extended nonlinear system can successfully be synchronized by imposed structures. The underlying mechanisms appear to be quite general. Therefore, similar synchronization—or rather *synchorization* (from $\chi\omega\rho\iota\omega\nu$: place)—phenomena should be observable in many other extended systems as well. Even though we demonstrated locking onto regular system states, the results give hope that synchorization of more complex states, i.e., of spatiotemporal chaos is also possible. Apart from the fundamental aspects, this would open the perspective for a realization of parallel secure data transmission, as proposed recently [63].

ACKNOWLEDGMENTS

This work would not have been possible without the support of T. Tschudi. The idea to apply the Farey construction goes back to F. Kaiser, who is acknowledged for a very helpful discussion about nonlinear resonances. We have strongly benefited from a collaboration with Jenoptik LOS GmbH, Jena, in the framework of a project funded by the Federal Ministry of Education and Research (BMBF) under Grant No. 13N7311/8. Jenoptik has kindly provided us liquid crystal light valves and the data projector. We particularly acknowledge the collaboration with P. Gussek.

[1] A. Pikovsky, M. Rosenblum, and J. Kurths, *Synchronization* (Cambridge University Press, Cambridge, 2001).

[2] G.D. VanWiggeren and R. Roy, Science **279**, 1198 (1998).

[3] P. Manneville, *Dissipative Structure And Weak Turbulence* (Academic Press, San Diego, 1990).

[4] M.C. Cross and P.C. Hohenberg, Rev. Mod. Phys. **65**, 851 (1993).

[5] D. Walgraef, *Spatio-temporal Pattern Formation* (Springer, New York, 1997).

[6] J. Opt. Soc. B **7** (6/7) (1990), special issue on transverse effects in nonlinear-optical systems, edited by N.B. Abraham and W.J. Firth; *Nonlinear Dynamics And Spatial Complexity In Optical Systems*, edited by R.G. Harrison and J.S. Uppal (SUSSP Publications, Edinburgh, 1992); Chaos, Solitons Fractals **4** (8, 9) (1994), special issue on nonlinear optical structures, patterns, chaos, edited by L. A. Lugiato; M.A. Vorontsov and W.B. Miller, *Self-organization in Optical Systems and Applications in Information Technology* (Springer, Berlin, 1995); Adv. At. Mol. Phys. **40**, 229 (1998), special issue on optical pattern formation, edited by L.A. Lugiato, M. Brambilla, and A. Gatti; Chaos, Solitons Fractals **10** (4-5) (1999), special issue on pattern formation in nonlinear optical systems, edited by R. Neubecker and T. Tschudi.

[7] R.E. Kelly and D. Pal, J. Fluid Mech. **86**, 433 (1978).

[8] H.R. Brand, Phys. Rev. A **32**, 3551 (1985).

[9] C. Elphick, J. Phys. A **19**, L877 (1986); P. Coullet and D. Repaux, Europhys. Lett. **3**, 573 (1987); E.M.F. Curado and C. Elphick, J. Phys. A **20**, 1205 (1987).

[10] P. Coullet, C. Elphick, and D. Repaux, Phys. Rev. Lett. **58**, 431 (1987).

[11] P. Coullet, Phys. Rev. Lett. **56**, 724 (1986).

[12] R. Schmitz and W. Zimmermann, Phys. Rev. E **53**, 5993 (1996).

[13] C. Utzny, W. Zimmermann, and M. Bär, Europhys. Lett. **57**, 113 (2002).

[14] L.M. Pismen, Phys. Rev. Lett. **59**, 2740 (1987).

[15] P. Coullet and D. Walgraef, Europhys. Lett. **10**, 525 (1989).

[16] P. Parmananda, Phys. Rev. E **56**, 1595 (1997).

[17] S. Boccaletti, J. Bragard, and F.T. Arecchi, Phys. Rev. E **59**, 6574 (1999); J. Bragard and S. Boccaletti, *ibid.* **62**, 6346 (2000).

[18] L. Junge and U. Parlitz, Phys. Rev. E **61**, 3736 (1999).

[19] D. Walgraef, Europhys. Lett. **7**, 485 (1988).

[20] O. Steinbock, V. Zykov, and S.C. Müller, Nature (London) **366**, 322 (1993).

[21] V. Petrov, Q. Ouyang, and H.L. Swinney, Nature (London) **388**, 655 (1997).

[22] A.L. Lin *et al.*, Phys. Rev. Lett. **84**, 4240 (2000).

[23] A.K. Horváth *et al.*, Phys. Rev. Lett. **83**, 2950 (1999); M. Dolnik, A.M. Zhabotinsky, and I.R. Epstein, Phys. Rev. E **63**, 026101 (2001).

[24] J. Wolff *et al.*, Science **294**, 134 (2001).

[25] V. Pérez-Muñuzuri *et al.*, Physica D **82**, 195 (1995).

[26] M. Lowe, J.P. Gollub, and T.C. Lubensky, Phys. Rev. Lett. **51**, 786 (1983); M. Lowe and J.P. Gollub, Phys. Rev. A **31**, 3893 (1985).

[27] G. Hartung, F.H. Busse, and I. Rehberg, Phys. Rev. Lett. **66**, 2742 (1991).

[28] O. Steinbock, P. Kettunen, and K. Showalter, Science **269**, 1857 (1995).

[29] M. Bär *et al.*, J. Phys. Chem. **100**, 19106 (1996).

[30] R.F. Ismagilov, D. Rosmarin, D.H. Gracias, and A.D. Stroock, Appl. Phys. Lett. **79**, 439 (2001).

[31] L. Kuhnert, Nature (London) **319**, 393 (1986); L. Kuhnert, K.I. Agladze, and V.I. Krinsky, *ibid.* **337**, 244 (1989).

[32] F. Fecher *et al.*, Chem. Phys. Lett. **313**, 205 (1999).

[33] M. Dolnik, I. Berenstein, A.M. Zhabotinsky, and I.R. Epstein, Phys. Rev. Lett. **87**, 238301 (2001).

[34] S. Kadar, J. Wang, and K. Showalter, Nature (London) **391**, 770 (1998).

[35] I. Sendina-Nadal *et al.*, Phys. Rev. Lett. **80**, 5437 (1998).

[36] M. Watzl and A.F. Münster, J. Phys. Chem. **102**, 2540 (1998).

[37] W. Zimmermann, B. Painter, and R. Behringer, Eur. Phys. J. B **5**, 757 (1998).

[38] G. D'Alessandro and W.J. Firth, Phys. Rev. Lett. **66**, 2597 (1991); G. D'Alessandro and W.J. Firth, Phys. Rev. A **46**, 537 (1992).

[39] R. Neubecker, G.-L. Oppo, B. Thuering, and T. Tschudi, Phys. Rev. A **52**, 791 (1995); B. Thüring *et al.*, Asian J. Phys. **7**, 453 (1998).

[40] R. Neubecker and E. Benkler, Phys. Rev. E **65**, 066206 (2002).

[41] R. Neubecker, B. Thüring, M. Kreuzer, and T. Tschudi, Chaos, Solitons Fractals **10**, 681 (1999).

[42] G. Schliecker and R. Neubecker, Phys. Rev. E **61**, R997 (2000).

[43] M.A. Vorontsov and A.Yu. Karpov, J. Mod. Opt. **44**, 439 (1997).

[44] S. Longhi, Phys. Rev. A **56**, 2397 (1997).

[45] P.Y. Wang, P. Xie, J.-H. Dai, and H.-J. Zhang, Phys. Rev. Lett. **80**, 4669 (1998); P.Y. Wang and P. Xie, Phys. Rev. E **61**, 5120 (2000).

[46] P.Y. Wang and M. Saffman, Opt. Lett. **24**, 1118 (1999); R. Meucci, A. Labate, M. Ciofini, and P.Y. Wang, Quantum Semiclassic. Opt. **10**, 803 (1998).

[47] Yu.D. Dumarevskii *et al.*, Sov. J. Quantum Electron. **14**, 493 (1984) [Kvantovaya Elektron. (Moscow) **11**, 730 (1984)]; *Spatial Light Modulator Technique*, edited by U. Efron (Marcel Dekker, New York, 1995); W.P. Bleha, Laser Focus/Electro-Optics **19**, 110 (1983), and references therein; N. Hawlitschek, P. Gärtner, P. Gussek, and F. Reichel, Exp. Tech. Phys. (Lemgo, Ger.) **40**, 199 (1994).

[48] W.J. Firth, J. Mod. Opt. **37**, 151 (1990); M. Le Berre, E. Ressayre, A. Tallet, and J.-J. Zondy, J. Opt. Soc. Am. B **7**, 1346 (1990); G. D'Alessandro and W.J. Firth, Phys. Rev. Lett. **66**, 2597 (1991); R. Macdonald and H.J. Eichler, Opt. Commun. **89**, 289 (1992); M. Tamburrini, M. Bonavita, S. Wabnitz, and E. Santamato, Opt. Lett. **18**, 855 (1993); M. A Vorontsov and W.J. Firth, Phys. Rev. A **49**, 2891 (1994); G. Grynberg, A. Maître, A. Petrossian, Phys. Rev. Lett. **72**, 2379 (1994); T. Ackemann, Y.A. Logvin, A. Heuer, and W. Lange, *ibid.* **75**, 3450 (1995); J. Glückstad and M. Saffman, Opt. Lett. **20**, 551 (1995); T. Honda and H. Matsumoto, *ibid.* **20**, 1755 (1995); T. Honda, H. Matsumoto, M. Sedlatschek, C. Denz, and T. Tschudi, Opt. Commun. **33**, 293 (1997).

[49] F.T. Arecchi, S. Bocaletti, S. Ducci, E. Pamapaloni, P.L. Ramazza, and S. Residori, J. Nonlinear Opt. Phys. Mater. **9**, 183 (2000).

[50] S.A. Akhmanov, M.A. Vorontsov, and V.Yu. Ivanov, JETP Lett. **47**, 707 (1988) [Pis'ma Zh. Éksp. Teor. Fiz. **47**, 611 (1988)]; S.A. Akhmanov *et al.*, J. Opt. Soc. Am. B **9**, 78 (1992); M.A. Vorontsov, N.G. Iroshnikov, and R.L. Abernathy, Chaos, Solitons Fractals **4**, 1701 (1994).

[51] E. Pampaloni, S. Residori, and F.T. Arecchi, Europhys. Lett. **24**, 647 (1993); P.L. Ramazza, S. Residori, E. Pamapaloni, and A.V. Larichev, Phys. Rev. A **53**, 400 (1996).

[52] S. Ducci, P.L. Ramazza, W. Gonzalez-Vinas, and F.T. Arecchi, Phys. Rev. Lett. **83**, 5210 (1999).

[53] B. Thüring, R. Neubecker, and T. Tschudi, Opt. Commun. **102**, 111 (1993); M.A. Vorontsov and W.J. Firth, Phys. Rev. A **49**, 2891 (1994); Y. Hayasaki, H. Yamamoto, and N. Nishida, Opt. Commun. **151**, 263 (1998).

[54] M.A. Vorontsov and A.Yu. Karpov, Opt. Lett. **20**, 2466 (1995); A. Schreiber, B. Thüring, M. Kreuzer, and T. Tschudi, Opt. Commun. **136**, 415 (1997); P.L. Ramazza, S. Ducci, S. Bocaletti, and F.T. Arecchi, J. Opt. B: Quantum Semiclassical Opt. **2**, 399 (2000).

[55] E. Benkler, M. Kreuzer, R. Neubecker, and T. Tschudi, Phys. Rev. Lett. **84**, 879 (2000); E. Benkler, M. Kreuzer, R. Neubecker, and T. Tschudi, J. Opt. A. Pure Appl. Opt. **2**, 303 (2000).

[56] R. Neubecker and A. Zimmermann, Phys. Rev. E **65**, 035205(R) (2002).

[57] R. Neubecker, A. Zimmermann, and O. Jakoby, Appl. Phys. B **76**, 383 (2003).

[58] R. Neubecker, Opt. Commun. **132**, 593 (1996).

[59] F. Kaiser (private communication).

[60] F. Kaiser, in *Vistas on Biorythmicity*, edited by H. Greppin, R. Degli Agosti, and M. Bonzon (University of Geneva, Geneva, Switzerland, 1996), p. 175.

[61] H.G. Schuster, *Deterministic Chaos* (VCH Verlag, Weinheim, 1989).

[62] M. Schroeder, *Fractals, Chaos, Power Laws* (W. H. Freeman, New York, 1991).

[63] J. García-Ojalvo and R. Roy, Phys. Rev. Lett. **86**, 5204 (2001).